Hindawi
International Journal of Antennas and Propagation
Volume 2022, Article ID 6151505, 14 pages
https://doi.org/10.1155/2022/6151505

Research Article

A Wideband Circularly Polarized Dielectric Resonator Antenna Using Inverse *f*-Shaped Slot Excitation with Parasitic Metal Structure

Zizu Chen, Guoliang Yu, Di Wu, Mingmin Zhu, Yang Qiu, and Hao-Miao Zhou

Key Laboratory of Electromagnetic Wave Information Technology and Metrology of Zhejiang Province, College of Information Engineering, China Jiliang University, Hangzhou 310018, China

Correspondence should be addressed to Yang Qiu; qiuyang@cjlu.edu.cn and Hao-Miao Zhou; zhouhm@cjlu.edu.cn

Received 9 March 2022; Revised 18 June 2022; Accepted 11 July 2022; Published 2 August 2022

Academic Editor: María Elena de Cos Gómez

In this paper, a single-fed wideband circularly polarized dielectric resonator antenna (DRA) is proposed. The antenna consists of a substrate, a cylindrical dielectric resonator, and four curved parasitic metal blocks that are rotated and placed around the dielectric resonator. The GND of the substrate is etched with an inverse *f*-shaped slot. The orthogonal working mode of the DRA is excited by the inverse *f*-shaped slot coupled to the microstrip, thereby obtaining circularly polarized radiation. The impedance bandwidth and axial ratio bandwidth of the antenna are improved by optimizing the structure of the inverse *f*-shaped slot and the shape and size of curved parasitic metal blocks, and finally, a circularly polarized dielectric resonator antenna with significant bandwidth advantages is obtained. The antenna is simulated, fabricated, and measured. The measured results show that the proposed circularly polarized DRA has an impedance bandwidth of 58.5% (2.61–4.77 GHz) and an axial bandwidth of 55.2% (2.75–4.85 GHz) and finally achieves an effective axial bandwidth of 53.7% (2.75–4.77 GHz), the peak gain of 6.84 dBi, and average efficiency of 90.78%, with excellent overall performance.

1. Introduction

With the rapid development of wireless communication technology, the increasing communication data and the complex and changeable communication environment put forward higher requirements for antenna bandwidth, gain, efficiency, and especially anti-interference ability. The dielectric resonator antenna (DRA) has no surface wave loss due to the use of nonmetallic material resonator radiation. Compared with traditional microstrip antennas, it has unique advantages such as low loss, wide bandwidth, and easy excitation, which makes it have an important application value in modern wireless communication systems [1, 2]. In particular, the circularly polarized DRA has the ability to suppress multipath interference and resist polarization mismatch [3, 4], which can improve the anti-interference ability of the antenna to guarantee the transmission quality of electromagnetic signals so that it has an ideal application prospect in radio frequency identification (RFID) system, global positioning system, and satellite communication/navigation system. Therefore, research on circularly polarized DRA has attracted increasing attention in recent years [5–10].

DRAs have many ways to achieve circularly polarized radiation. For example, multifeed technology adjusts the phase by introducing couplers, phasers, or power dividers, to obtain the electric field component with orthogonal polarization and realize circular polarization [11–14]. However, the introduction of couplers, phasers, and power divider makes the feed network complex and the antenna size larger [15]. In addition, multifeed technology also needs to ensure high isolation between feed network ports; otherwise, it will seriously reduce the axial ratio bandwidth of the antenna [16]. On the contrary, the single-feed technology has more advantages in the feed structure, and its methods of realizing circular polarization can be roughly divided into

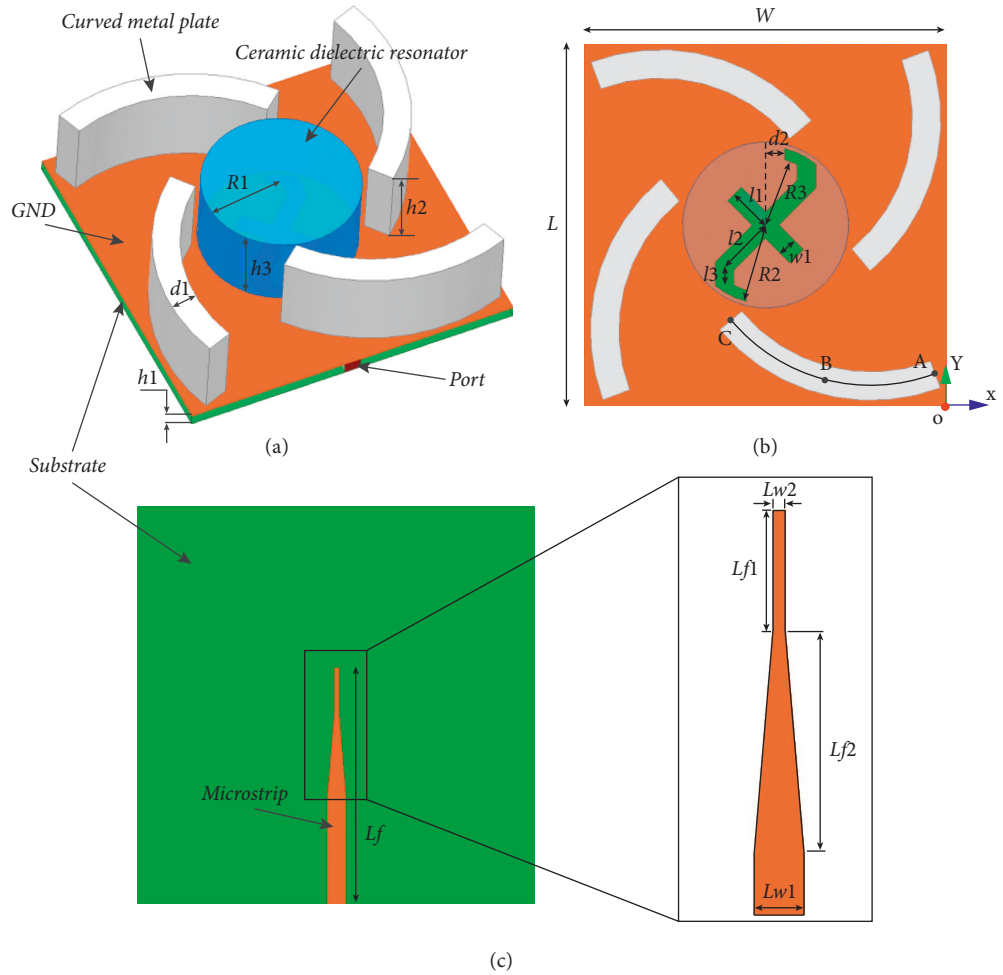

Figure 1: The geometry of the proposed antenna: (a) 3D structure, (b) top view, and (c) bottom view.

four categories: exciting special shape resonators [5, 17], parasitic metal structures [6, 18], multiresonator layout [7, 10], and special slot structures [8, 19, 20]. Usually, dielectric resonators are hard ceramic materials, and it is hard to cut and grind them into complex special shapes and process parasitic metal structures on their surfaces [8]. In addition, the introduction of too many parasitic metal structures on the surface of the resonator will reduce the gain and impedance bandwidth, affecting the performance of the antenna [21]. Using a multiple resonator layout often requires stacking multiple resonators, increasing the number of antenna layers, and making the antenna structure complex [22].

The DRA with a special slot structure can be achieved only by substrate, special slot structure, and dielectric resonator due to the simple slot processing technology; moreover, the simple antenna structure also has a favorable application prospect. In reference [8], a circularly polarized DRA for WLAN applications is achieved by etching four rectangular slots with a 30° rotation distribution on the GND, but the impedance bandwidth is only 26.7% and the axial ratio bandwidth is only 23.6%. References [19, 20], respectively, use the slot structure of unequal-length cross slot and Archimedes spiral slot, combined with a dielectric resonator to realize the circular polarization, but the effective axial ratio bandwidth is less than 26%. Therefore, it is still challenging to design a wideband circularly polarized DRA with a simple structure and good performance by using a special slot coupling structure.

Firstly, a simple cylindrical dielectric resonator is selected and placed on the substrate etched with a coupling slot on the GND in this paper. The orthogonal working mode of the DRA is excited by the microstrip-coupled slot to achieve circular polarization radiation. Then, to improve the impedance bandwidth and axial ratio bandwidth of the DRA, four curved parasitic metal blocks are placed around the cylindrical dielectric resonator, and their shape and size are optimized. To further ensure a higher effective axial ratio bandwidth, the impedance bandwidth and the axial ratio bandwidth can be highly overlapped, and the slot on the GND of the substrate is optimized and evolved into an inverse *f*-shaped slot. Finally, a simple wideband circularly polarized DRA is obtained, and the measured results show that its effective axial ratio bandwidth is as high as 2.75–4.77 GHz.

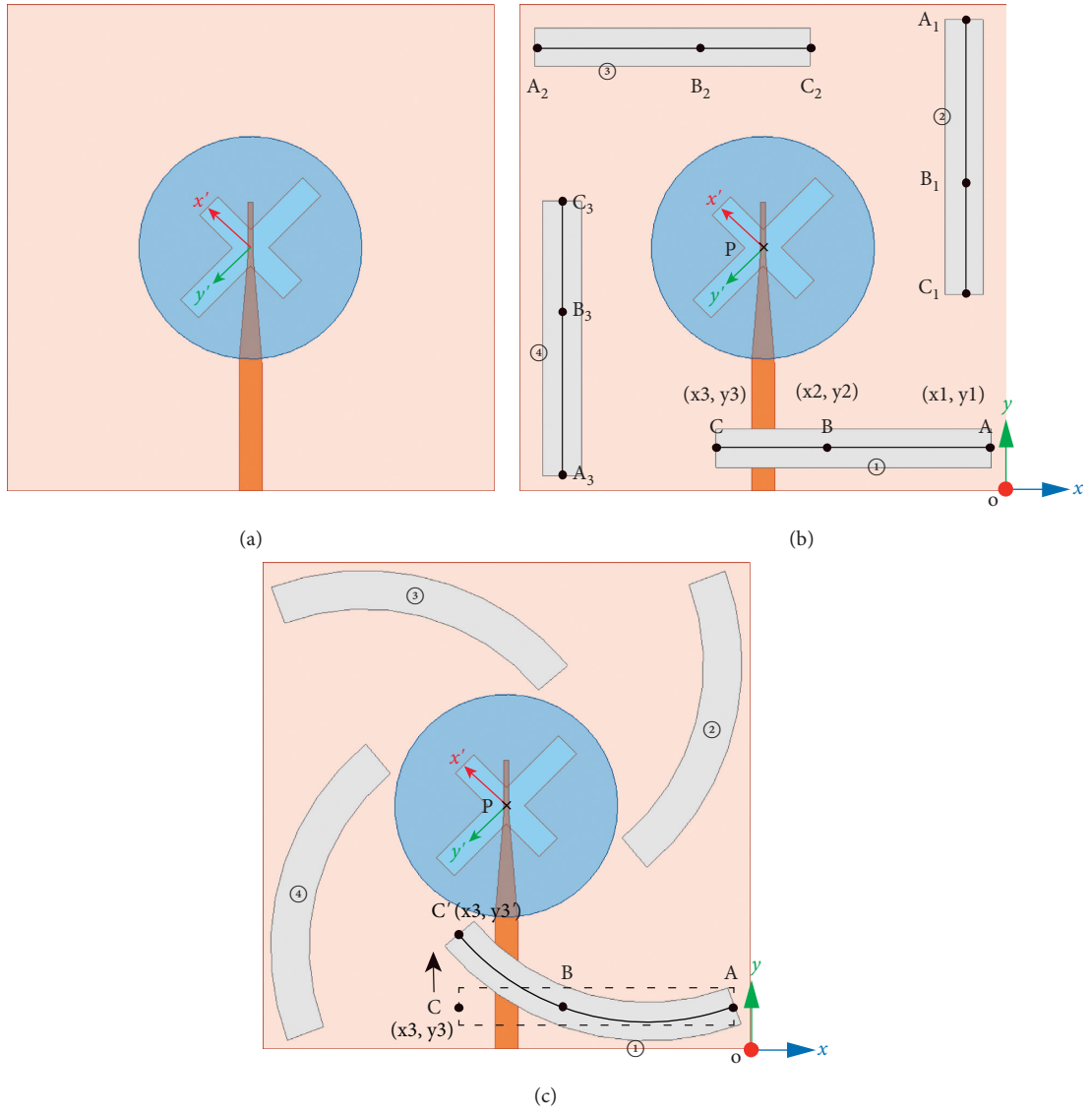

FIGURE 2: The top view of the reference antenna structure: (a) Ref. 1, (b) Ref. 2, and (c) Ref. 3.

2. Antenna Design

2.1. Antenna Structure. The 3D structure of the wideband circularly polarized DRA proposed in this paper is shown in Figure 1(a). The antenna is composed of three parts: a cylindrical ceramic dielectric resonator, four curved metal blocks, and a substrate. The material of the antenna substrate is FR4 ($\varepsilon_r = 4.4$ and $\tan\delta = 0.02$), with a thickness of $h1$. The upper surface of the substrate is the GND, and the inverse f-shaped slot is etched on the GND. A cylindrical resonator with a radius of $R1$ and a height of $h3$ is placed in the center above the substrate, and its material is Al_2O_3 ceramics ($\varepsilon_r = 9.5$). Four curved metal blocks with a thickness of $d1$ and a height of $h2$ are rotated and placed around the resonator, which are made of aluminum alloy and attached to the PCB through conductive adhesive, so as to ensure a good conductive path between the metal blocks and the PCB. Figure 1(b) is a top view of the antenna; the centrosymmetric inverse f-shaped coupling slot is etched into the GND. The inverse f-shaped coupling slot evolves from the basic unequal-length cross-coupling slot. A single curved metal block is determined by three points A, B, and C, and their coordinates are $(x1, y1)$, $(x2, y2)$, and $(x3, y3')$, respectively. The other three metal blocks can be positioned by rotating the single curved metal block by 90°, 180°, and 270° around the center point of the substrate. The overall size of the antenna is $L \times W$. Figure 1(c) is the bottom view of the antenna. A microstrip with a length of Lf is located on the midline of the lower surface of the substrate, which is wider at the bottom and narrower at the top. The rectangle box is an enlarged view of this area. The microstrip adopts a Balun structure, and its bottom and top are set to different widths, which are mainly used to adjust the impedance matching in order to obtain a wider impedance bandwidth. The port is

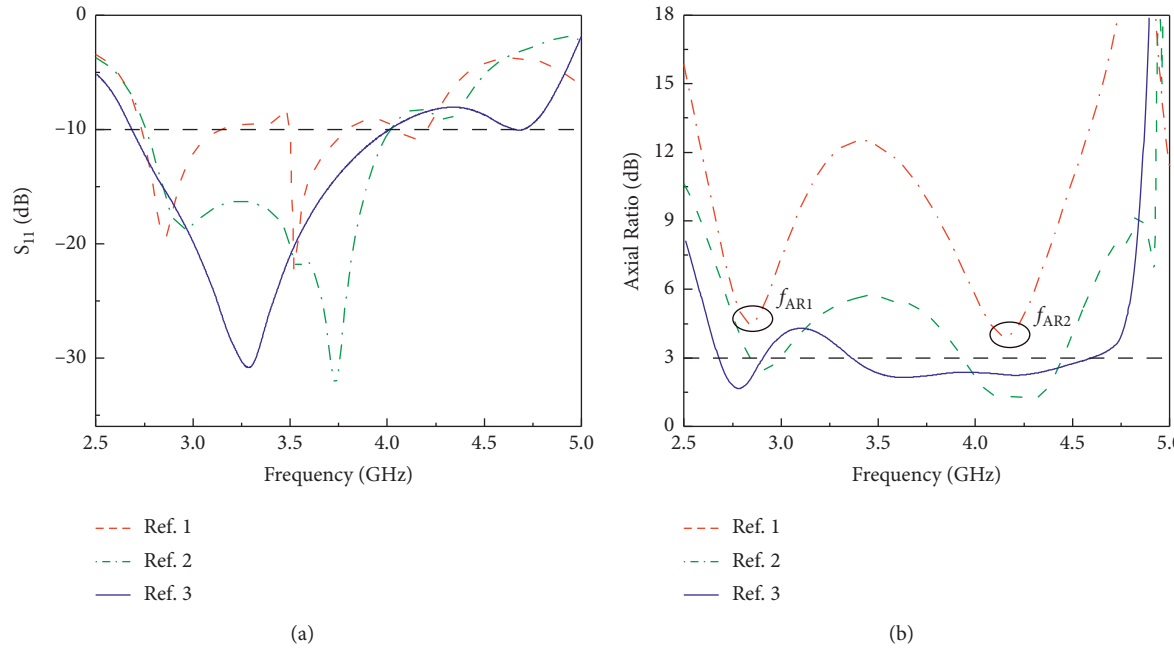

FIGURE 3: Simulation results of S_{11} and the axial ratio of reference antenna: (a) S_{11} and (b) axial ratio.

located on the side of the substrate and is connected to the microstrip on the lower surface of the substrate and the GND on the upper surface of the substrate, which feeds the resonator by coupling between the microstrip and the slot.

2.2. Antenna Design Process. In circularly polarized DRA, the unequal-length cross slot is a common coupling structure that can excite circularly polarized waves. Therefore, the coupling structure of the basic antenna in this paper also chooses the unequal-length cross slot; see the Ref. 1 structure shown in Figure 2(a). The simulation result of return loss (S_{11}) of the Ref. 1 antenna is shown in Figure 3(a), and its −10 dB impedance bandwidths are 2.74–3.14 GHz, 3.50–3.78 GHz, and 4.06–4.22 GHz, with relatively narrow overall bandwidths. The axial ratio simulation result of the Ref. 1 antenna is shown in Figure 3(b), and it can be seen from the figure that the antenna generates two axial ratio resonance points f_{AR1} at 2.84 GHz and f_{AR2} at 4.16 GHz, and their corresponding values are 4.5 dB and 3.9 dB, respectively.

The circularly polarized antenna requires an axial ratio of less than 3 dB, but the Ref. 1 antenna does not meet this requirement. Therefore, in order to lower the antenna axial ratio, four rotatably placed rectangular metal blocks are introduced into the Ref. 1 antenna to obtain the Ref. 2 antenna, whose structure is shown in Figure 2(b). The relative position of the no. 1 metal block on the substrate is determined by the three points A, B, and C on the center line, and their coordinates are ($x1$, $y1$), ($x2$, $y2$), and ($x3$, $y3$), respectively. Rotate the no. 1 metal block around the P point (the center point of the substrate) counterclockwise by 90°, 180°, and 270°, respectively, to determine the position of the nos. 2, 3, and 4 metal blocks. The axial ratio simulation results of the Ref. 2 antenna are shown as a green dotted line in Figure 4. Obviously, after the introduction of four rectangular metal blocks, the two axial ratio resonance points f_{AR1} and f_{AR2}, which were originally greater than 3 dB, were lowered to 2.48 dB and 1.22 dB, respectively, thus obtaining the 3 dB axial ratio band of 2.83–2.99 GHz (5.5%) and 3.94–4.45 GHz (12.1%); the circular polarization characteristics of the antenna are significantly improved. In order to explain the mechanism of loading rectangular metal blocks to improve the circular polarization of the antenna, we analyze the current of rectangular metal blocks. Figures 4(a) and 4(b) show the current distribution of the rectangular metal blocks at the axial ratio resonance point f_{AR1} (2.84 GHz). It can be seen from Figure 4(a) that at phase = 0° of resonance point, the currents of nos. 1 and 3 metal blocks are both along the negative direction of the x-axis, while the currents of nos. 2 and 4 metal blocks are, respectively, along the positive and negative directions of the z-axis. Because the currents of nos. 2 and 4 metal blocks are in opposite directions, the induced electric fields generated by them will resist each other, while the currents of nos. 1 and 3 metal blocks are in the same direction, and the induced electric fields will be superimposed on each other. Therefore, at phase = 0°, the induced electric field generated by the metal blocks current is mainly along the negative direction of x-axis. However, at the 90° phase, the currents of the metal blocks changed; the currents of nos. 1 and 3 the metal blocks became positive and negative directions along the z-axis, respectively, while the currents of the metal blocks nos. 2 and 4 became along the negative direction of the y-axis, as shown in Figure 4(b). Similarly, the electric field generated by the metal blocks current at the 90° phase is mainly along the negative direction of the y-axis. The x-axis and the y-axis are orthogonal, so a pair of orthogonal polarization fields with a

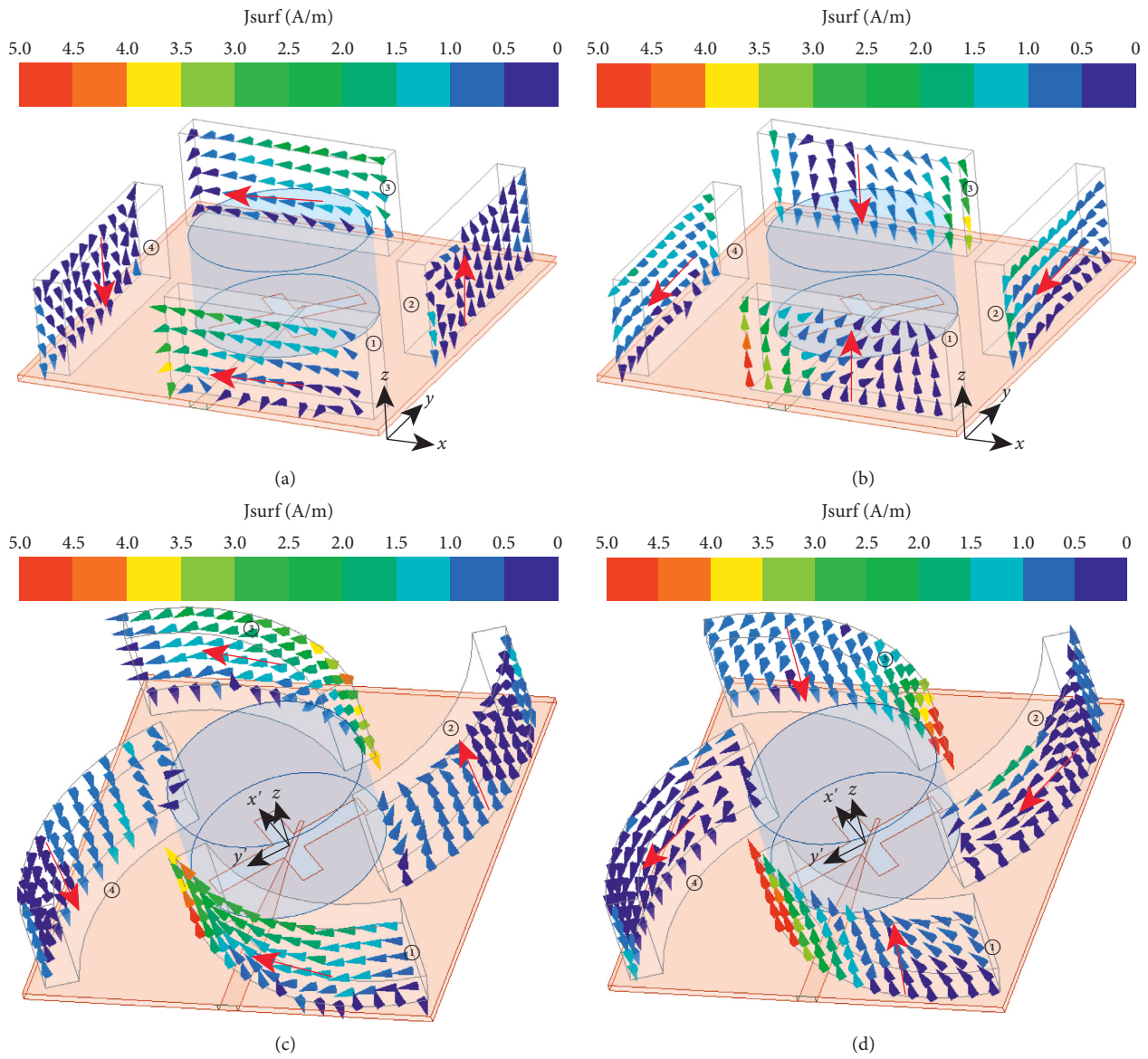

FIGURE 4: The current distribution of the metal blocks at the axial ratio resonance point f_{AR1} (2.84 GHz): (a) rectangular metal blocks and phase = 0°, (b) rectangular metal blocks and phase = 90°, (c) curved metal blocks and phase = 0°, and (d) curved metal blocks and phase = 90°.

phase difference of 90° can be obtained, thereby improving the circular polarization of the antenna.

Although the Ref. 2 antenna achieves 5.5% and 12.1% dual-frequency axial ratio passbands compared to the Ref. 1 antenna, the axial ratio bandwidth is still relatively narrow. In order to further widen the bandwidth of the axial ratio, the structure of the rectangular metal block needs to be optimized. Take no. 1 metal block as an example, keep the coordinates of point A and point B on the center line of no. 1 metal block unchanged, and only increase the y-axis coordinate $y3$ of point C so that point C is gradually moved up to point C' so that the rectangular metal becomes curved. Similarly, the Ref. 3 antenna can be obtained by performing similar operations on nos. 2, 3, and 4 metal blocks, as shown in Figure 2(c). Figure 5 shows the influence of the S_{11} and the axial ratio of the antenna when the key coordinate $y3$ changes. It can be seen that the change of $y3$ has little effect on the impedance bandwidth but has a significant impact on the axial ratio bandwidth. Figure 5(b) shows the axial ratio simulation results of $y3$ increasing from 5.5 mm to 13.5 mm in steps of 2 mm. When $y3$ gradually increases, the rectangular metal block gradually becomes curved; the value of the first axial ratio resonance point f_{AR1} gradually lowers; and the 3 dB axial ratio bandwidth of the second axial ratio resonance point f_{AR2} gradually widens. When $y3$ increases from 5.5 mm to 11.5 mm, the axial ratio bandwidth increases gradually. When $y3$ is 11.5 mm, the axial ratio bandwidth reaches the maximum value of 10.6% (2.68–2.98 GHz) and 35.0% (3.42–4.87 GHz), which is significantly better than the Ref. 1 antenna. However, when $y3$ continues to increase to 13.5 mm, the axial ratio bandwidth is 8.3% (2.66–2.89 GHz) and 29.2% (3.34–4.48 GHz), which is smaller than that when

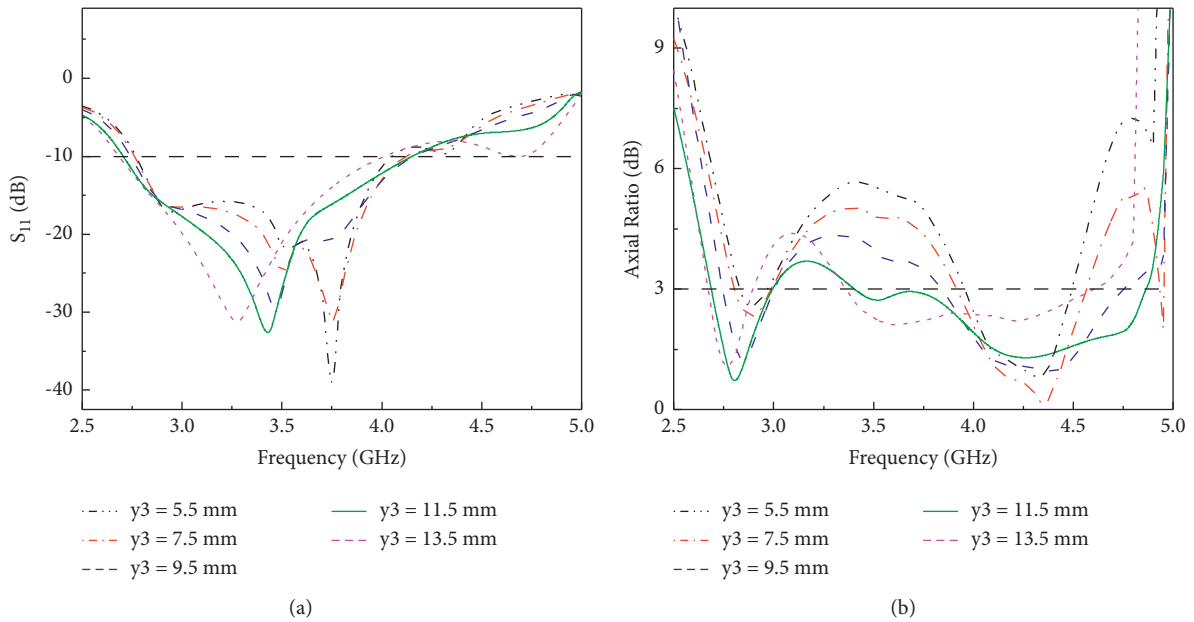

Figure 5: Simulation results of S_{11} and the axial ratio of different y_3: (a) S_{11} and (b) axial ratio.

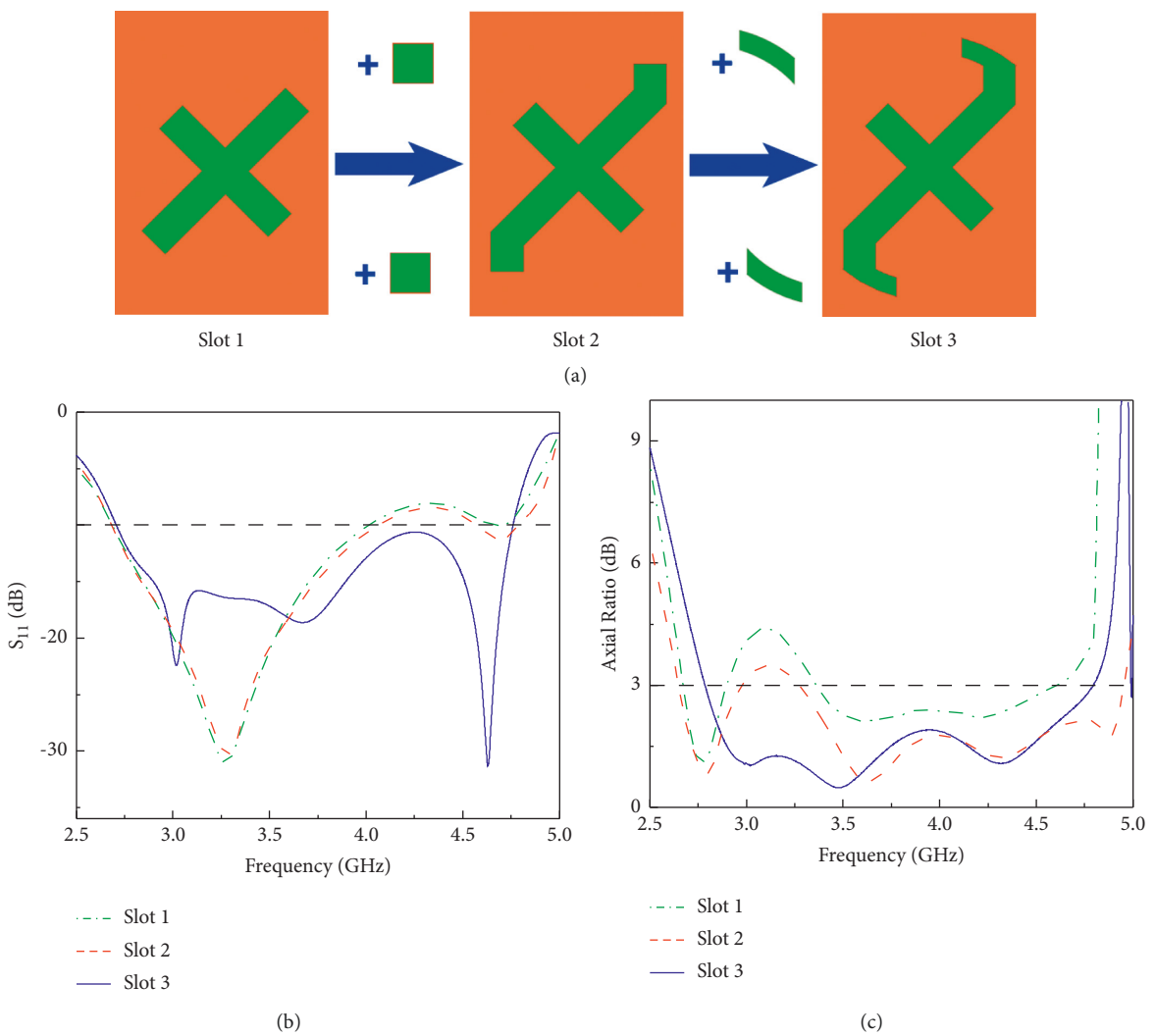

Figure 6: Schematic diagram of slot evolution and simulation results: (a) slot evolution, (b) S_{11}, and (c) axial ratio.

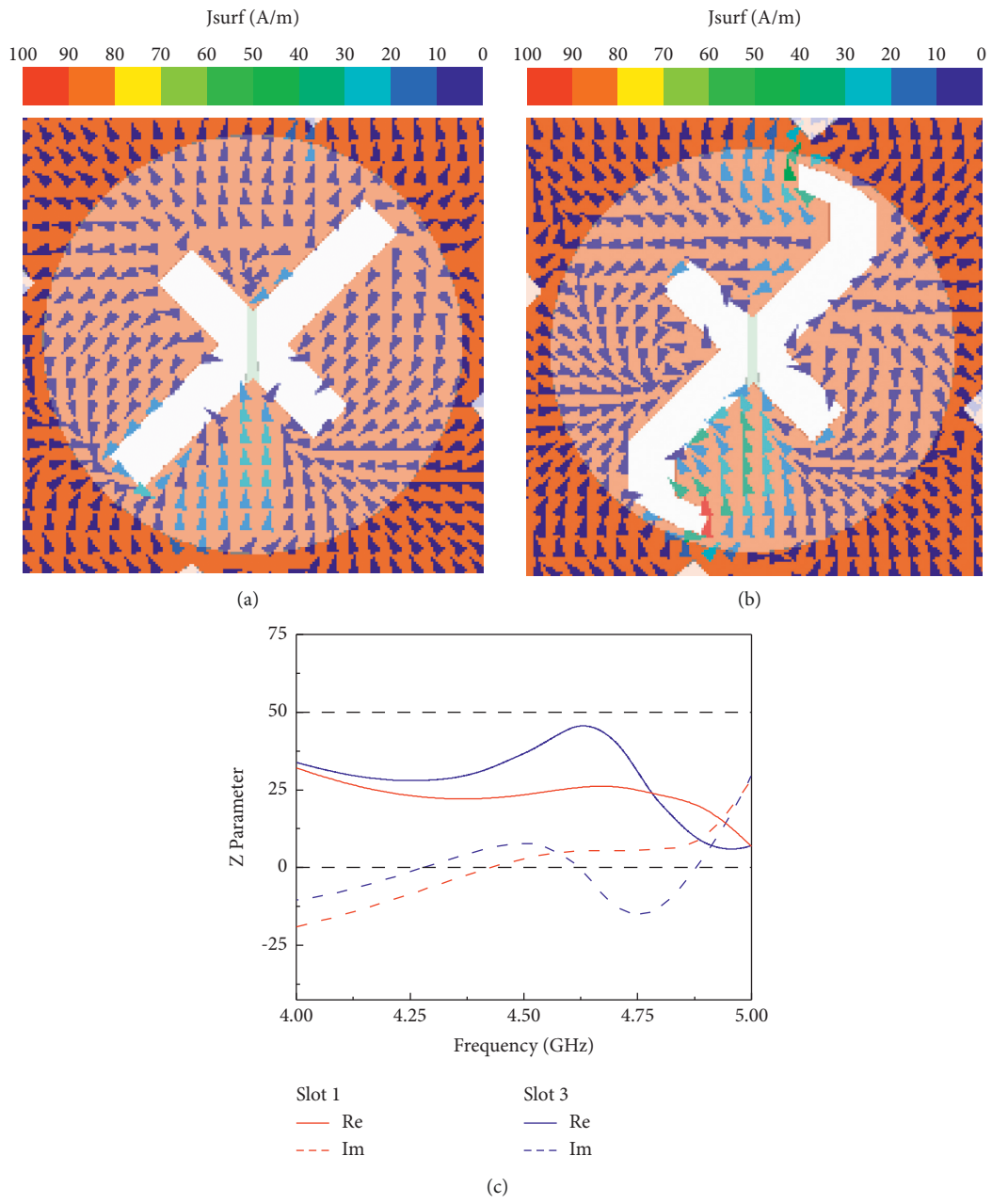

Figure 7: (a) GND surface current distribution of slot 1, (b) GND surface current distribution of slot 3, and (c) Z parameter simulation results.

$y3$ is 11.5 mm. Therefore, when using the unequal-length cross slot excitation, the $y3$ of the curved metal blocks is 11.5 mm.

The mechanism of loading curved metal blocks to improve the circular polarization of the antenna is similar to that of loading rectangular metal blocks mentioned above. Essentially, the curved metal blocks are only obtained by optimizing the parameters of the rectangular metal blocks. Figures 4(c) and 4(d) show the current distribution of the curved metal blocks at 0° phase and 90° phase. It can be seen from the figure that the current distribution of the curved metal blocks is similar to that of the rectangular metal blocks, and a pair of orthogonal polarization fields with a phase difference of 90° can also be obtained. Meanwhile, compared with the rectangular metal blocks, the curved metal blocks are closer to the dielectric resonator, and the induced current inside them is stronger, so the pair of orthogonal polarization fields generated are also stronger, so as to further improve the circular polarization of the antenna.

In designing a wideband circularly polarized DRA, it is not enough to ensure a wide impedance bandwidth and a wide axial ratio bandwidth. It is also necessary to achieve a high overlap of the impedance bandwidth and the axial ratio bandwidth, that is, to ensure a highly effective axial ratio bandwidth. For example, the Ref. 3 antenna in Figure 2 has an impedance bandwidth of 37.0% (2.74–4.02 GHz) and a

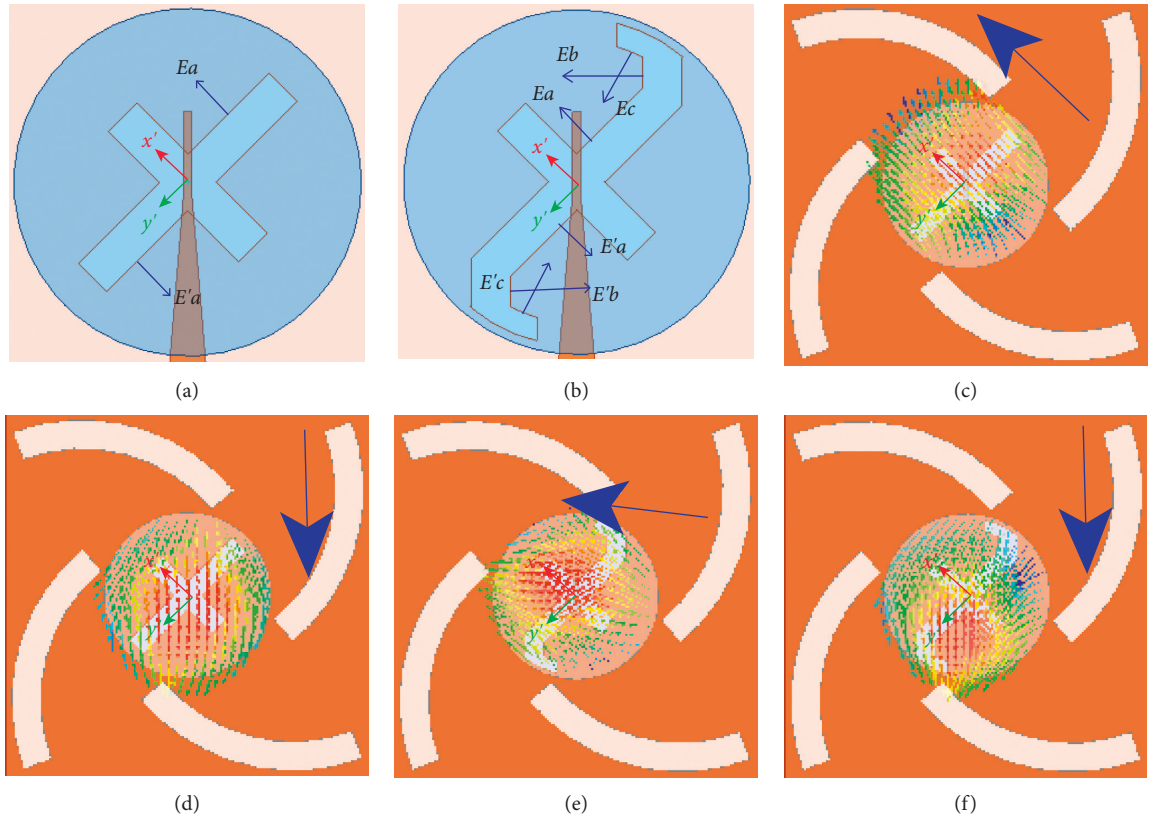

Figure 8: Schematic diagram of electric field excited by slot and electric field distribution on the top surface of dielectric resonator: (a) electric field excited by slot 1, (b) electric field excited by slot 3, (c) slot 1 and phase = 0°, (d) slot 1 and phase = 90°, (e) slot 3 and phase = 0°, and (f) slot 3 and phase = 90°.

dual-frequency axial ratio bandwidth of 8.3% (2.66–2.89 GHz) and 29.2% (3.34–4.48 GHz), but its effective axial ratio bandwidth is only 5.3% (2.74–2.89 GHz) and 18.5% (3.34–4.02 GHz). This is attributed to the Ref. 3 antenna in the 2.89–3.34 GHz band, and the return loss meets the −10 dB requirement, but the axial ratio does not meet the 3 dB requirement for circular polarization. In addition, in the 4.02–4.48 GHz band, the axial ratio is lower than the 3 dB required by circular polarization, but the return loss is not lower than the −10 dB required by the impedance bandwidth. To obtain a wider effective axial ratio bandwidth, based on the Ref. 3 antenna, its slot structure is shown in slot 1 of Figure 6(a), and the unequal-length cross slot is redesigned. Firstly, a pair of rectangular slots are, respectively, introduced up and down the long slot of the unequal-length cross slot, and the obtained slot structure is shown in slot 2 of Figure 6(a). Compared with slot 1, the impedance bandwidth of antenna with slot 2 does not change significantly, but its axial ratio bandwidth is significantly improved; see red dotted lines in Figures 6(b) and 6(c). And then, a pair of curved slots are introduced based on slot 2 to obtain the final designed inverse *f*-shaped slot, as shown in slot 3 of Figure 6(a). As can be seen from the blue lines in Figures 6(b) and 6(c), after introducing a pair of curved slots, a new −10 dB impedance bandwidth is obtained in the 4.02–4.76 GHz band, and a new 3 dB axial ratio bandwidth is obtained in the 2.89–3.34 GHz band. Finally, the impedance bandwidth of 55.2% (2.70–4.76 GHz), the axial ratio bandwidth of 53.3% (2.78–4.80 GHz), and the effective axial ratio bandwidth of 52.5% (2.78–4.76 GHz) are obtained.

The current distribution is an important factor affecting the working characteristics of the antenna. In order to explain the reason for the increase of impedance bandwidth, Figures 7(a) and 7(b) show the GND surface current distribution of antenna with Slot 1 and antenna with Slot 3 at 4.63 GHz, respectively. It can be seen that after slot 1 is transformed into slot 3, the current intensive area is generated at the head and tail of the inverse *f*-shaped slot, and the current direction is changed; the current path is extended so that the real part of the impedance increases, which is closer to 50Ω in 4.02–4.76 GHz (see Figure 7(c)). As a result, the antenna impedance matching is improved, and the impedance bandwidth is significantly improved, reaching 55.2% (2.70–4.76 GHz).

When the longer slot in the unequal-length cross slot is coupled with the microstrip, the electric field in the *Ea* direction inside the dielectric resonator will be excited, as shown in Figure 8(a). When the unequal-length cross slot turns into the inverse *f*-shaped slot, as shown in Figure 8(b), two electric fields in the *Eb* and *Ec* directions will be additionally excited, and these two electric fields will interact with the electric field in the Ea direction, making the overall electric field direction is rotated counterclockwise by some

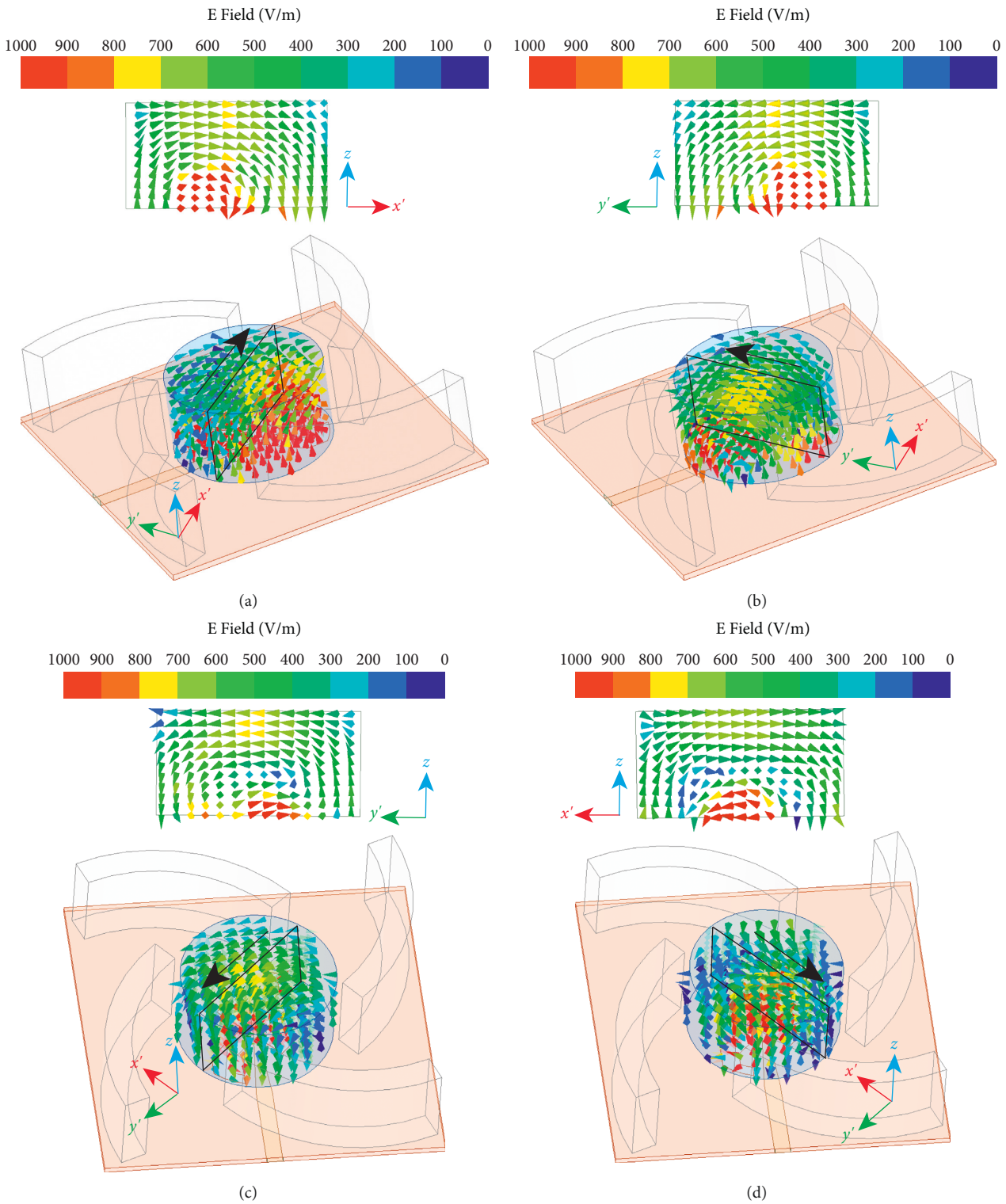

Figure 9: Simulated electric field vector distributions inside dielectric resonator (DR) and its corresponding principal plane with different phases: (a) at 3.00 GHz and phase = 0°, (b) at 3.00 GHz and phase = 90°, (c) at 4.25 GHz and phase = 0°, and (d) at 4.25 GHz and phase = 90°.

angles. To explain the widening of the axial ratio bandwidth, Figures 8(c)–8(f) shows the electric field distribution on the upper surface of the dielectric resonator at 3.15 GHz. At phase = 0°, the electric field excited by unequal-length cross slot is mainly along the x' direction, while the electric field excited by inverse f-shaped slot is rotated counterclockwise by some angles. At phase = 90°, the electric fields excited by unequal-length cross and inverse f-shaped slots are approximately in the same direction. With the different phases (0° and 90°), the electric field excited by the inverse f-shaped

Table 1: Design parameters of the proposed antenna.

Parameter	Value	Parameter	Value	Parameter	Value
W	57 mm	$l1$	6.92 mm	$Lw2$	0.63 mm
L	57 mm	$l2$	9.12 mm	$x1$	−1.8
$R1$	13.05 mm	$l3$	3 mm	$y1$	5
$d1$	4.5 mm	$R2$	12.4 mm	$x2$	−22
$h1$	1 mm	$R3$	10.67 mm	$y2$	5
$h2$	14.6 mm	Lf	33.81 mm	$x3$	−34
$h3$	13.5 mm	$Lf1$	6.31 mm	$y3$	13.5
$d2$	3 mm	$Lf2$	12.5 mm		
$w1$	3 mm	$Lw1$	2.7 mm		

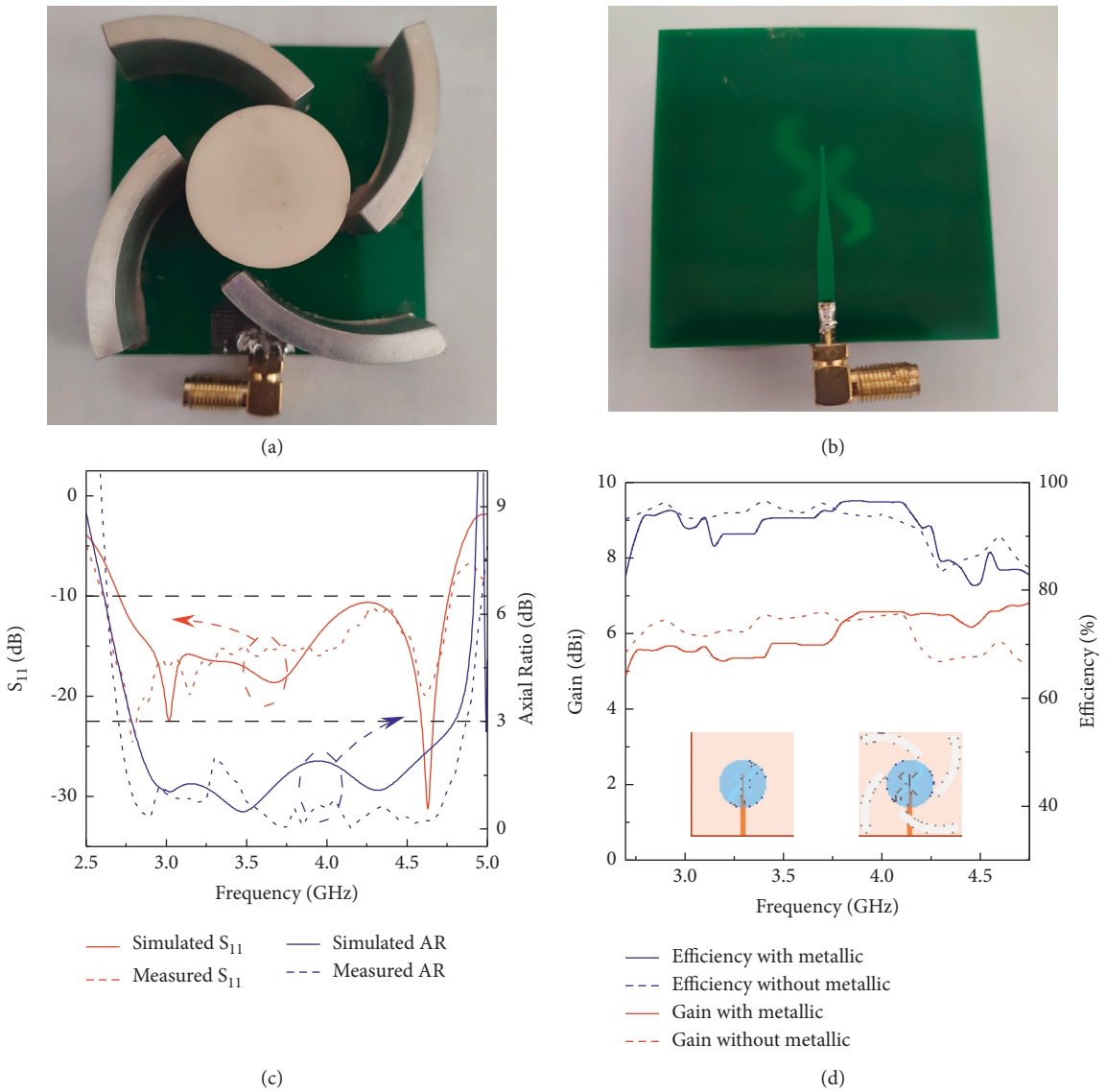

Figure 10: (a) Top view of the proposed antenna, (b) bottom view of the proposed antenna, (c) simulated and measured results of S_{11} and axial ratio, and (d) measured gain and efficiency of the antenna with and without metal blocks.

is closer to the orthogonal field than that of the unequal-length cross slot. As a result, the axial ratio value of antenna drops at 3.15 GHz, and the two separate axial ratio bands are merged into one, which widens the axial ratio bandwidth to 53.3% (2.78–4.80 GHz). Finally, an effective axial ratio bandwidth of 52.5% (2.78–4.76 GHz) is obtained.

In order to further verify the working mechanism of circularly polarized DRA, Figure 9 shows the electric field

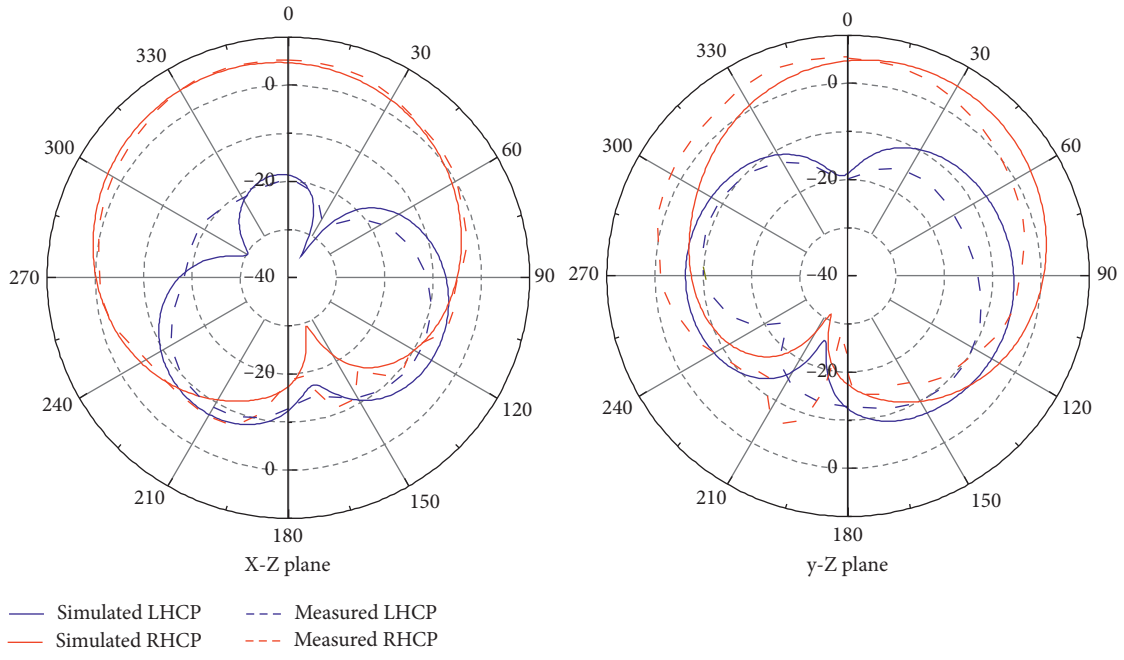

(a)

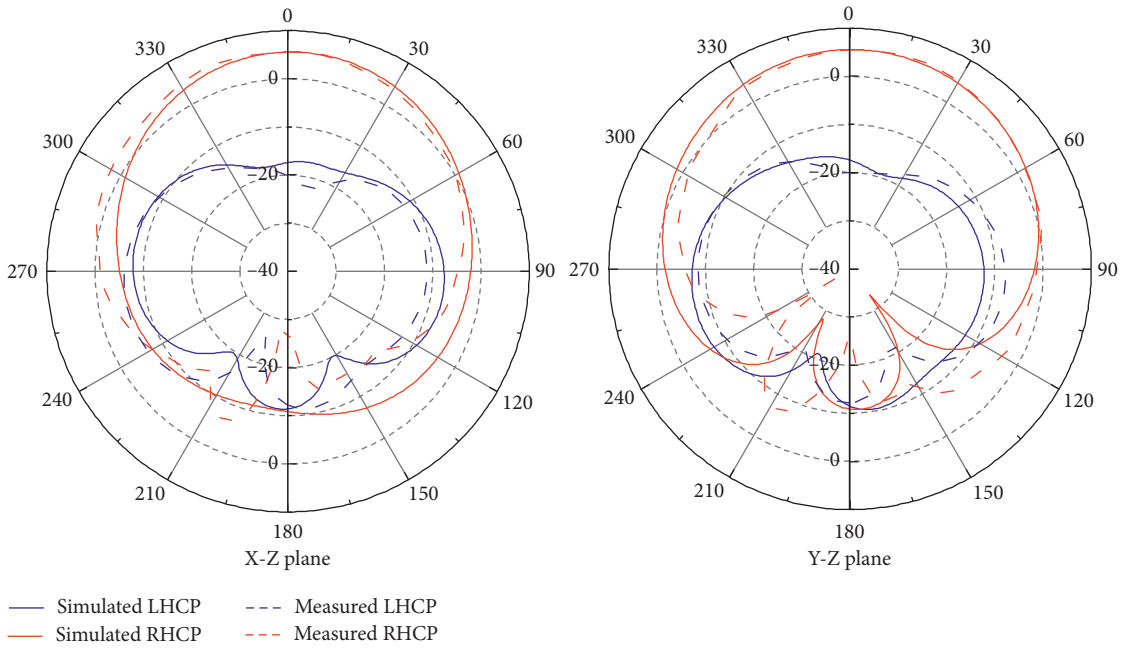

(b)

Figure 11: Continued.

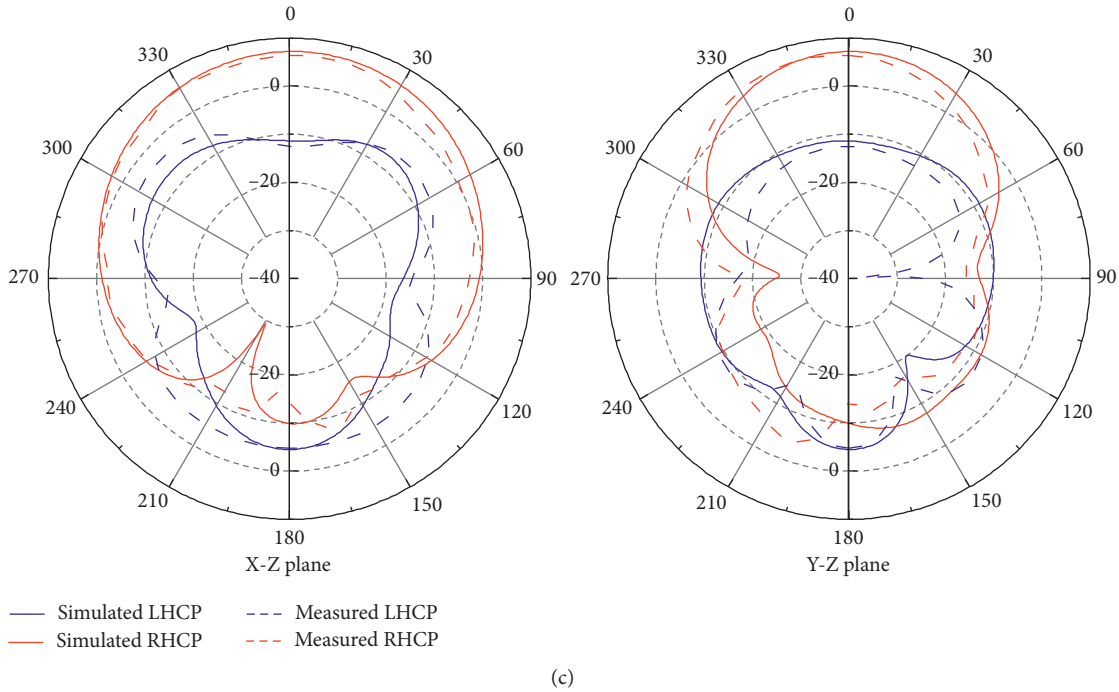

(c)

Figure 11: Simulated and measured radiation patterns of the proposed antenna: (a) 3.01 GHz, (b) 3.68 GHz, and (c) 4.63 GHz.

distribution inside the dielectric resonator of DRA proposed in this paper at two axial ratio resonance points f_{AR1} (3.00 GHz) and f_{AR2} (4.25 GHz). It can be seen from Figures 9(a) and 9(b) that at 3.00 GHz, the excited mode is the fundamental mode HEM_{111}. At 0° phase, the electric field vector is along the x′ direction, while at the 90° phase, the electric field vector is along y′ direction. The axial ratio resonance point at 3.00 GHz is generated due to this pair of orthogonal degenerate modes HEM_{111} (x') and HEM_{111} (y'). As can be seen from Figures 9(c) and 9(d), at 4.25 GHz, the excitation mode is high-order mode HEM_{113}. At the 0° phase, the electric field vector is along y' direction, while at the 90° phase, the electric field vector is along the negative direction of the x'-axis. This pair of orthogonal degenerate modes HEM_{113} (x') and HEM_{113} (y') produce the axial ratio resonance point at 4.25 GHz.

3. Results and Discussion

After the optimization design of the wideband circularly polarized DRA structure proposed in this paper, the final structure size is obtained, as shown in Table 1. The actual antenna is fabricated according to this size, and the front and back of the antenna are shown in Figures 10(a) and 10(b), respectively. The return loss was obtained by testing with an Agilent N5230C vector network analyzer, and the axial ratio, gain, and efficiency were obtained by testing in SATIMO microwave anechoic chamber. Figure 10(c) shows the comparison between the simulated results and the measured results of the antenna S_{11} parameters and axial ratio. As can be seen from the figure, the simulated and measured impedance bandwidths are 2.70–4.76 GHz and 2.61–4.77 GHz, respectively, and the simulated and measured axial ratio bandwidths are 2.78–4.80 GHz and 2.75–4.85 GHz, respectively. In general, the measured results are basically the same as the simulated results, and the deviations are mainly caused by the permittivity deviation of the resonator material and the manual welding process. Figure 10(d) shows the measured gain and efficiency of the antenna with and without metal blocks. It can be seen that the average gain of the antenna with metallic blocks is 5.5 dBi in the band of 2.70–3.75 GHz, the average gain is 6.5 dBi in the band of 3.75–4.77 GHz, and the peak gain is 6.84 dBi. The average gain of the antenna without metallic blocks is 6.2 dBi in the band of 2.70–3.75 GHz, which is higher than that of the antenna with metallic blocks; the average gain is 5.8 dBi in the band of 3.75–4.77 GHz, which is lower than that of the antenna with metallic blocks; and the peak gain is 6.56 dBi. In the working frequency band, the average radiation efficiency of the antenna with metallic blocks is 90.78%, while the average radiation efficiency of the antenna without metallic blocks is 91.9%. In general, loading metallic blocks will have some effect on antenna gain and efficiency, but the effect is not very obvious.

Figure 11 shows the simulated and measured results of the radiation patterns (xz plane and yz plane) of the proposed antenna at 3.01 GHz, 3.68 GHz, and 4.63 GHz. The measured results are in good agreement with the simulated results. The right-hand circularly polarized (RHCP) field component is significantly larger than the left-hand circularly polarized field (LHCP) component at the three frequency points, and the proposed antenna is a right-hand circularly polarized DRA, as can be seen from the figure. The pattern is relatively stable in the entire working bandwidth,

Table 2: Comparison of the proposed antenna with existing works.

Ref.	−10 dB IBW (GHz)	3 dB AR BW (GHz)	Effective AR BW (%)	Gain (dBi)	Feeding type
[5]	69.7% (2.90–6.00 GHz)	44.7% (3.68–5.80 GHz)	44.7	6.3	Microstrip line
[6]	20.3% (3.59–4.40 GHz)	21.1% (3.60–4.45 GHz)	20.0	6.5	Microstrip line
[7]	36.0% (4.00–5.80 GHz)	26.0% (4.40–5.70 GHz)	26.0	7.7	Microstrip line
[8]	26.7% (5.25–6.87 GHz)	23.6% (5.42–6.87 GHz)	23.6	3.4	Slot couple
[9]	46.9% (2.20–3.50 GHz)	49.5% (2.20–3.70 GHz)	46.9	4.7	Slot couple
[10]	49.7% (4.20–6.80 GHz)	41.0% (4.30–6.70 GHz)	41.0	1.5	Slot couple
This work	58.5% (2.61–4.77 GHz)	55.2% (2.75–4.85 GHz)	53.7	6.8	Slot couple

and the radiation is mainly along the positive direction of the z-axis, indicating that the antenna is a perfect unidirectional radiation antenna. Table 2 presents a comparison of the measured results between the proposed antenna and the published wideband circularly polarized DRA. As can be seen from Table 2, the antenna proposed in this paper has the highest axial ratio bandwidth and effective axial ratio bandwidth, which is only second to [5] in impedance bandwidth and [7] in gain, with outstanding wideband characteristics.

4. Conclusion

In this paper, a novel wideband circularly polarized DRA is obtained by placing a cylindrical dielectric resonator in the center of a substrate etched with an inverse f-shaped on the GND and rotated by positing four curved metal blocks around the resonator. Since the ceramic dielectric resonator is a simple cylindrical shape, complex cutting, and grinding processes are not required. The antenna is simple in structure, easy to manufacture, and has splendid application prospects. Simulated and measured results show that the antenna has high impedance bandwidth, axial ratio bandwidth, and effective axial ratio bandwidth. Compared with the existing wideband circularly polarized DRA, the proposed antenna has the best effective axial ratio bandwidth, excellent comprehensive performance, and favorable practical value.

Data Availability

The data that support the findings of this study are available from the corresponding author upon reasonable request.

Conflicts of Interest

The authors declare that they have no conflicts of interest.

Authors' Contributions

Zizu Chen and Guoliang Yu contributed equally to this work.

Acknowledgments

This study was supported by the Natural Science Foundation of Zhejiang Province under Grand nos. LZ19A020001, LQ19F010005, and LY21F010011 and the Funds of the National Natural Science Foundation of China under Grand nos. 11972333, 51902300, and 11902316. The authors would like to express their sincere appreciation for these supports.

References

[1] Z. Chen, H. Wong, and Y. Liu, "A polarizer integrated dielectric resonator antenna for polarization reconfigurability," *IEEE Transactions on Antennas and Propagation*, vol. 67, no. 4, pp. 2723–2728, 2019.

[2] Y. X. Sun, K. W. Leung, and J. F. Mao, "Dualfunction dielectric resonator as antenna and phase-delay-line load: designs of compact circularly polarized/differential antennas," *IEEE Transactions on Antennas and Propagation*, vol. 66, no. 1, pp. 414–419, 2018.

[3] X. C. Wang, L. Sun, X. L. Lu, S. Liang, and W. Z. Lu, "Single-feed dual-band circularly polarized dielectric resonator antenna for CNSS applications," *IEEE Transactions on Antennas and Propagation*, vol. 65, no. 8, pp. 4283–4287, 2017.

[4] Y. T. Liu, K. W. Leung, J. Sun, and Y. X. Sun, "Linearly and circularly polarized filtering dielectric resonator antennas," *IEEE Transactions on Antennas and Propagation*, vol. 67, no. 6, pp. 3629–3640, 2019.

[5] S. Trinh-Van, Y. Yang, K. Y. Lee, and K. C. Hwang, "Single-fed circularly polarized dielectric resonator antenna with an enhanced axial ratio bandwidth and enhanced gain," *IEEE Access*, vol. 8, pp. 41045–41052, 2020.

[6] J. Iqbal, U. Illahi, M. I. Sulaiman et al., "Bandwidth enhancement and generation of CP by using parasitic patch on rectangular DRA for wireless applications," *IEEE Access*, vol. 7, pp. 94365–94372, 2019.

[7] W. J. Sun, W. W. Yang, L. Qin, W. Chen, and J. X. Chen, "A circularly polarized dielectric resonator antenna and its reconfigurable design," *IEEE Antennas and Wireless Propagation Letters*, vol. 19, no. 7, pp. 1088–1092, 2020.

[8] R. Kumari, R. K. Gangwar, and R. K. Chaudhary, "Investigation on rotated rectangular slots to improve the circular polarization in cylindrical dielectric resonator antenna," *IEEE Access*, vol. 9, pp. 97327–97336, 2021.

[9] M. Yang, Y. Pan, and W. Yang, "A singly fed wideband circularly polarized dielectric resonator antenna," *IEEE Antennas and Wireless Propagation Letters*, vol. 17, no. 8, pp. 1515–1518, 2018.

[10] G. Varshney, V. S. Pandey, R. S. Yaduvanshi, and L. Kumar, "Wide band circularly polarized dielectric resonator antenna with stair-shaped slot excitation," *IEEE Transactions on Antennas and Propagation*, vol. 65, no. 3, pp. 1380–1383, 2017.

[11] M. Rad, N. Nikkhah, B. Yazdi, and M. Yazdi, "Wideband dielectric resonator antenna with dual circular polarization," *IEEE Transactions on Antennas and Propagation*, vol. 70, no. 1, pp. 714–719, 2022.

[12] W. Liu, Z. Cao, and Z. Wang, "A wideband circularly polarized dielectric resonator antenna array," *IEEE Access*, vol. 99, p. 1, 2020.

[13] R. Han, S. Zhong, and J. Liu, "Broadband circularly polarised dielectric resonator antenna fed by wideband switched line coupler," *Electronics Letters*, vol. 50, no. 10, pp. 725-726, 2014.

[14] E. H. Lim, K. W. Leung, and X. S. Fang, "The compact circularly-polarized hollow rectangular dielectric resonator antenna with an underlaid quadrature coupler," *IEEE Transactions on Antennas and Propagation*, vol. 59, no. 1, pp. 288–293, 2011.

[15] A. Seo and M. Seo, "Size-reduction of a dual-band circularly polarized dielectric resonator antennas," *IEEE Access*, vol. 9, pp. 126457–126465, 2021.

[16] C. X. Mao, Z. H. Jiang, D. H. Werner, S. S. Gao, and W. Hong, "Compact self-diplexing dual-band dual-sense circularly polarized array antenna with closely spaced operating frequencies," *IEEE Transactions on Antennas and Propagation*, vol. 67, no. 7, pp. 4617–4625, 2019.

[17] R. Chowdhury and R. K. Chaudhary, "An approach to generate circular polarization in a modified cylindrical-shaped dielectric resonator antenna using PMC boundary approximation," *IEEE Antennas and Wireless Propagation Letters*, vol. 17, no. 9, pp. 1727–1731, 2018.

[18] Y. M. Pan and K. W. Leung, "Wideband omnidirectional circularly polarized dielectric resonator antenna with parasitic strips," *IEEE Transactions on Antennas and Propagation*, vol. 60, no. 6, pp. 2992–2997, 2012.

[19] A. A. Abdulmajid, Y. Khalil, and S. Khamas, "Higher-order-mode circularly polarized two-layer rectangular dielectric resonator antenna," *IEEE Antennas and Wireless Propagation Letters*, vol. 17, no. 6, pp. 1114–1117, 2018.

[20] M. Zou, J. Pan, and Z. Nie, "A wideband circularly polarized rectangular dielectric resonator antenna excited by an archimedean spiral slot," *IEEE Antennas and Wireless Propagation Letters*, vol. 14, pp. 446–449, 2015.

[21] S. Gotra, G. Varshney, R. S. Yaduvanshi, and V. S. Pandey, "Dual-band circular polarisation generation technique with the miniaturisation of a rectangular dielectric resonator antenna," *IET Microwaves, Antennas & Propagation*, vol. 13, no. 10, pp. 1742–1748, 2019.

[22] W. J. Sun, W. W. Yang, P. Chen, and J. X. Chen, "Design of a wideband circularly polarized stacked dielectric resonator antenna," *IEEE Transactions on Antennas and Propagation*, vol. 67, no. 1, pp. 591–595, 2019.